Magneto-optical Kerr spectroscopy of (Ga,Mn)(As,P) ferromagnetic layers: Experiments and k.p theory

M Yahyaoui, H Riahi, A A Maaref, K Boujdaria, Aristide Lemaître, L. Thevenard, Catherine Gourdon

Magneto-optical Kerr spectroscopy of (Ga,Mn)(As,P) ferromagnetic layers: Experiments and k.p theory

M. Yahyaoui, H. Riahi, M. A. Maaref, K. Boujdaria, A. Lemaître, L. Thevenard, and C. Gourdon

Citation: Journal of Applied Physics **121**, 125702 (2017); doi: 10.1063/1.4979205
View online: http://dx.doi.org/10.1063/1.4979205
View Table of Contents: http://aip.scitation.org/toc/jap/121/12
Published by the American Institute of Physics

Magneto-optical Kerr spectroscopy of (Ga,Mn)(As,P) ferromagnetic layers: Experiments and k.p theory

M. Yahyaoui,[1] H. Riahi,[2] M. A. Maaref,[2] K. Boujdaria,[1,a)] A. Lemaître,[3] L. Thevenard,[4] and C. Gourdon[4]

[1]*Laboratoire de Physique des Matériaux: Structure et Propriétés, Faculté des Sciences de Bizerte, Université de Carthage, 7021 Zarzouna, Bizerte, Tunisia*
[2]*Laboratoire Matériaux Molécules et Applications, IPEST, Université de Carthage, La Marsa, Tunisia*
[3]*Centre de Nanosciences et de Nanotechnologies, CNRS, Univ. Paris-Sud, Université Paris-Saclay, F-91460 Marcoussis, France*
[4]*Sorbonne Universités, UPMC Univ Paris 06, CNRS-UMR 7588, Institut des NanoSciences de Paris, F-75005 Paris, France*

(Received 7 December 2016; accepted 14 March 2017; published online 28 March 2017)

We present a theoretical and experimental study of the magneto-optical properties of thin (Ga,Mn)(As,P) layers on GaAs substrates with varying phosphorus fractions. Using a 40-band **k.p** model as well as an antiferromagnetic (*s*, *p*)-*d* exchange interaction, we calculate the dielectric tensor, the Kerr rotation angle, and the ellipticity in the interband transition region. Our calculations are validated through a set of accurate comparisons with experimental results. The Kerr ellipticity peak is found to be 2 to 3 times larger than the Kerr rotation angle both experimentally and theoretically. This work will enable to optimize the magneto-optical effects in these layers for maximum sensitivity in ultra-fast magnetization dynamics and domain microscopy experiments. *Published by AIP Publishing.*
[http://dx.doi.org/10.1063/1.4979205]

I. INTRODUCTION

Among diluted magnetic semiconductors (SCs) based on III-V compounds, $Ga_{1-x}Mn_xAs_{1-y}P_y$ has attracted much attention over the past decade.[1–6] Introducing a few percents of phosphorus (P) at the arsenic sites in $Ga_{1-x}Mn_xAs$ layers offers an interesting additional degree of freedom to adjust properties such as the Curie temperature, the magnetic anisotropy, the band gap, or the carrier concentration.[1,2] Moreover, this quaternary alloy contains much fewer defects than (Ga,Mn)As.[7]

Magneto-optical (MO) spectroscopy is widely used both in the x-ray domain and in the visible range as a powerful tool for investigating the interplay between magnetic ordering and electronic structure in ferromagnetic materials with either itinerant or localized spins.[8–10] The magneto-optical Kerr effect (MOKE) describes the change of the polarization state of light when reflected off a magnetic material. It arises from the transverse dielectric function proportional to the magnetization *M*. Depending on the chosen experimental configuration, a sensitivity to its out of plane (polar Kerr effect) or in-plane (longitudinal Kerr effect) components can be obtained. In the ferromagnetic SC (Ga,Mn)As, MO spectroscopy in the visible and infrared spectral regions has been used to gain insight into the controversial issue of the energy position of the Fermi level, inside the valence band (VB) or in an impurity band detached from the VB.[11–16] The prediction and experimental determination of MO spectra are also of prime importance to select the optimal wavelength for the optical investigation of static and dynamical magnetic properties. Optically detected hysteresis cycles obtained from the MOKE provide information on the magnetic anisotropy and magnetization reversal processes.[17] Using the time-resolved MOKE, laser pump-probe experiments enable the investigation of magnetization dynamics in the femtosecond to nanosecond range, in particular, the coherent collective magnetic excitations.[6,18,19] Magneto-optical microscopy uses the MOKE to gain insight into the magnetic domains static pattern[7,20,21] and the domain wall dynamics.[22]

While the MO effects in (Ga,Mn)As have been extensively investigated,[13–16,23–34] the MO properties of (Ga,Mn)(As,P) thin films, more specifically the interplay between the Mn doping and P substitution, remain to be investigated. Hence, in the present study, we report on the MOKE in the interband transition range for ferromagnetic (Ga,Mn)(As,P) samples with different P and Mn contents. The dielectric functions and MOKE spectra are obtained using the electronic band structure (BS) of $Ga_{1-x}Mn_xAs_{1-y}P_y$/GaAs layers determined in the framework of the 40-band **k.p** model.[35] This model has been successfully used to investigate the magnetic properties of (Ga,Mn)(As,P) thin films under various conditions of strain, P and carrier concentrations.[36,37] An excellent agreement with experimental results was obtained. In particular, the values of the magnetic anisotropy constants, especially the out-of-plane uniaxial and in-plane biaxial anisotropy constants, were well reproduced. In the present work, the good quantitative agreement of our calculated MOKE spectra with experimental data further confirms that our theoretical approach accurately models the multiband electronic structure of (Ga,Mn)(As,P).

II. SAMPLES AND BAND STRUCTURE

A. Samples

$Ga_{1-x}Mn_xAs_{1-y}P_y$ layers were grown by molecular beam epitaxy on a GaAs substrate. Two sets of samples were

a)kais.boujdaria@fsb.rnu.tn

TABLE I. Ga_{1-x} Mn_xAs_{1-y} P_y sample parameters: the phosphorus concentration [P], the nominal Mn content [Mn], the perpendicular strain component s_{zz}, the saturation magnetization M_S at T = 4 K, the effective Mn concentration x_{eff}, the splitting parameter of the valence subbands B_G,[38] the estimated carrier density p, and Fermi energy E_F.

Sample	A	B	C	D
[P] (%)	0	7.0	11.3	11.3
[Mn] (%)	7.0	7.0	7.0	10.2
s_{zz} (%)	0.23	−0.16	−0.31	−0.32
M_S (emu cm^{-3})	37.6	39.2	35	53.8
x_{eff}(%)	3.7	3.8	3.5	5.2
B_G(meV)	−26.0	−27.5	−24.7	−49.4
p (10^{19} cm^{-3})	5.6	5.6	3.2	12.4
E_F(meV)	−110	−110	−81	−130

prepared, with nominal Mn concentration 7% and 10%, respectively, and with P concentration ranging from 0% to 18%. The layer thickness is 50 ± 5 nm. The samples were annealed 1 h at 250 °C, which is known to increase the hole concentration, hence the Curie temperature,[38] by out-diffusion of interstitial Mn acting as double donors. The magnetic anisotropy was qualitatively checked by magneto-transport measurements. Samples were processed into Hall bars and the longitudinal and transverse resistivities were measured as a function of the perpendicular magnetic field. The saturation magnetization and the Curie temperature were obtained from superconducting quantum interference device (SQUID) magnetometry and the anisotropy constants from ferromagnetic resonance experiments.[39] The effective Mn concentration x_{eff} is obtained from the saturation magnetization at $T = 4$ K. For the x = 7% series, samples with P concentration below (above) 4%–5% have an in-plane (out-of-plane) magnetic easy axis.[2] For the x = 10% series, the in-plane/out-of-plane transition is around y = 5%–6%. For the present study, we choose to compare three samples from the x = 7% series (A, B, and C) with different P concentrations and two samples (C and D), one from each series, with the same P concentration. The characteristics of the studied samples and the parameters used in the calculation are summarized in Table I. Figures 1(a) and 1(b) show the magnetization curves obtained from SQUID measurements and the hysteresis cycles obtained from magneto-transport, respectively. At low temperature, samples B, C, and D have a perpendicular-to-plane easy axis and sample A an in-plane easy axis (Fig. 1(b)).

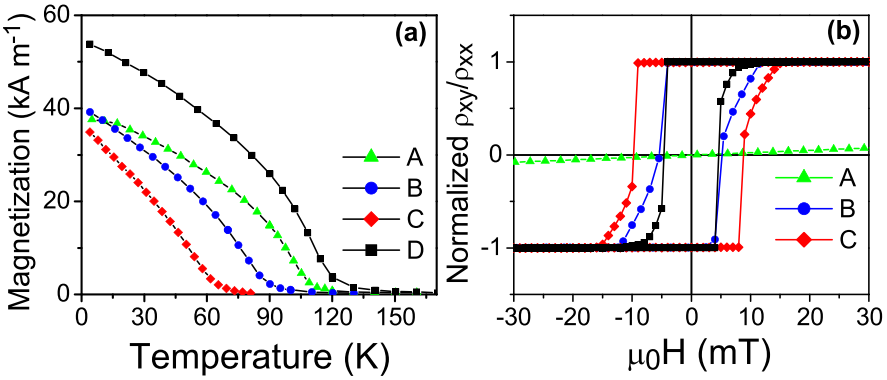

FIG. 1. (a) Magnetization as a function of the temperature for samples A, B, C, and D. (b) Hysteresis cycles obtained from the ratio of the transverse Hall resistivity ρ_{xy} to the longitudinal one ρ_{xx} under perpendicular-to-plane applied magnetic field at $T = 16$ K for samples B, C, and D and $T = 4$ K for sample A. ρ_{xy}/ρ_{xx} is proportional to M_z.

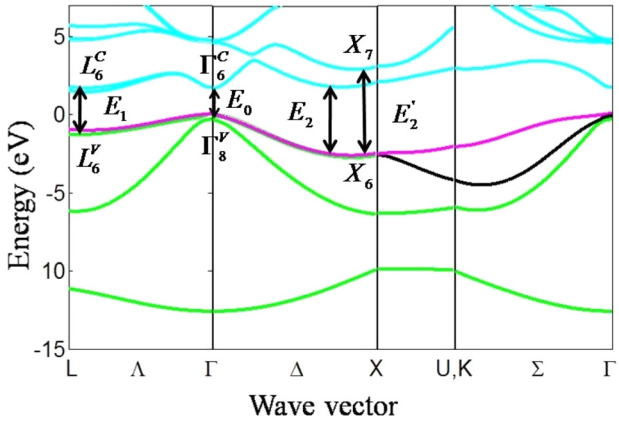

FIG. 2. Band structure of (Ga,Mn)(As,P) in sample C along the high symmetry lines of the first Brillouin zone and relevant critical point optical transitions.

B. Band structure

To obtain the dependence of the MO properties as a function of P and Mn fractions, we first need to calculate the band structure (BS) of $(Ga_{1-x}Mn_x)(As_{1-y}P_y)$ compounds using the $\mathbf{k}\cdot\mathbf{p}$ theory. Our theoretical model description starts by coupling the BS of bulk SCs calculated using a 40-band $\mathbf{k}\cdot\mathbf{p}$ model[35,40] with $S = 5/2$ Mn local moments using a semi-phenomenological local exchange interaction treated in the mean-field approximation.[38,41] In our calculations, we take into account the epitaxial strain which is modeled using the Bir-Pikus Hamiltonian.[42] Our model is identical in all respects to the one detailed in Ref. 37. Therefore, we do not reproduce here all the complicated orbital basis, energy level structures, band-edge energies, and matrix elements, instead referring the reader to Refs. 35, 37, and 40.

Since we are interested in the optical properties of highly p-doped $(Ga_{1-x}Mn_x)(As_{1-y}P_y)$ compounds, we have to take into account the band gap renormalization. Indeed, the large concentration of free carriers ($>10^{19}$ cm^{-3}) in these compounds leads to a significant reduction of the band gap and inter-VB splittings.[43–45] This effect known as the band gap narrowing (BGN) originates from the exchange and correlation contributions to the electron-electron interactions. We qualitatively take into account the BGN by shifting rigidly the hole-occupied exchange spin-split bands by an amount $2.6 \times 10^{-8} p^{1/3}$ eV (Refs. 29 and 46) with p in cm^{-3}. The values of p are computed for the chosen Fermi energy based on the 40-band **k.p** model (Table I).

An example of the BS calculated with the full Hamiltonian **H** for $x_{\text{eff}} = 0.035$ and $y = 0.113$ is shown in Fig. 2. The electronic BS of this compound shows features similar to that of bulk GaAs. The band diagram is well reproduced on a width of about 18 eV.

The 40-band $\mathbf{k} \cdot \mathbf{p}$ method has some important advantages over the 8-band Hamiltonian (two-level model with s (p) states for the conduction (valence) band), which is often employed to calculate the electronic BS of $(III_{1-x}\ Mn_x)V$ SCs. Contrary to the 8-band Hamiltonian, the 40-band **k.p** method is known to be valid up to 6 eV above and 12 eV below the top of the VB in four directions, namely, ΓX, ΓL, ΓK, and XU. Hence, as shown in Ref. 37, a satisfactory agreement between the two models is obtained only up to $k \sim 0.1\ \text{Å}^{-1}$ measured from the Γ edge. When calculating the dielectric permittivity and the spectral dependence of the MOKE of $(Ga_{1-x}\ Mn_x)(As_{1-y}\ P_y)$ in the interband transition region, the deviation of the 8-band **k.p** model band diagram from the real BS might lead to an inaccurate estimation of the optical properties of these materials. Furthermore, one has to keep in mind that within the two-level **k.p** model, one needs to specify the Luttinger parameters to take into account the interaction of the VB with remote bands. This can be achieved for (Ga,Mn)As by taking the parameters of GaAs but these parameters are not available for $(Ga_{1-x}\ Mn_x)(As_{1-y}\ P_y)$. In addition, we have shown that the more accurate description of the magnetic properties of bulk (Ga,Mn)(As,P) originates from a better description of the bands with the 40-band **k.p** model, in particular, from a good determination of the Luttinger parameters.[37] Thus, a full calculation of the BS and an accurate determination of Luttinger parameters are essential for modeling the optical properties of these materials, which cannot be achieved with the 8-band **k.p** model.

III. MAGNETO-OPTICAL KERR EFFECT

A. Methodology

Using the linear response theory, the elements of the interband dielectric tensor are given by[30]

$$\varepsilon_{\alpha\beta} = \delta_{\alpha\beta} + \frac{e^2\hbar^2}{m_0^2\varepsilon_0}\frac{1}{(2\pi)^3} \times \sum_{c,v}\int\int\int_{BZ}(f_v - f_c)\frac{1}{(E_{cv})^2} \times \left[\frac{p_{vc}^{\alpha}p_{cv}^{\beta}}{E_{cv} - i\hbar\gamma - \hbar\omega} + \frac{p_{cv}^{\alpha}p_{vc}^{\beta}}{E_{cv} + i\hbar\gamma + \hbar\omega}\right]dk_x dk_y dk_z, \tag{1}$$

where c and v label the conduction and valence bands, respectively. The subscripts α and β denote the coordinates. $E_{cv} = E_c(k) - E_v(k)$, $p_{vc}^{\alpha} = \langle vk|p_{\alpha}|ck\rangle$ and $p_{cv}^{\beta} = \langle ck|p_{\beta}|vk\rangle$ are components of the momentum matrix element between states of bands c and v with crystal momentum k, $\hbar\omega$ is the photon energy, and $\hbar\gamma$ is the lifetime broadening. Our procedure to evaluate the momentum matrix elements involved in optical transitions is similar to the approach developed in Ref. 47. f_c and f_v are the Fermi-Dirac distribution functions. At zero temperature and positive $\hbar\omega$ the difference $(f_v - f_c)$ restricts v to occupied quasiparticle states ($f_v = 1$) and c to empty quasiparticle states ($f_c = 0$). The strong (s,p)-d exchange between the holes and Mn spins in diluted magnetic SCs causes the splitting of bands, which gives rise to a large off-diagonal dielectric function ε_{xy} related to spin-dependent optical transitions. In cubic or tetragonal crystals, ε_{xy} contains by symmetry a term proportional to M_z, the perpendicular-to-plane component of the magnetization, that gives rise to circular dichroism/birefringence (MOKE and Faraday effect) and a generally much smaller term proportional to M_xM_y related to linear dichroism/birefringence.[48] Here, we will only consider a magnetization vector parallel to z.

Due to the presence of charge compensating defects in $Ga_{1-x}Mn_xAs_{1-y}P_y$ samples depending on growth conditions, the position of the Fermi level in ferromagnetic $Ga_{1-x}Mn_xAs_{1-y}P_y$ is difficult to determine. Hence, for reasons of simplicity and lack of data on the hole concentration, we have assumed that the position of the Fermi level is at −110 meV from the top of the VB for samples A and B, −81 meV for sample C, and −130 meV for sample D. Using these values, we could obtain a good agreement between the calculated and experimental magnetic anisotropies.[37] The k_{α} ($\alpha = x, y, z$) integrals in Eq. (1) are extended over the first Brillouin zone (BZ) using the full BS calculated in Ref. 37.

In (Ga,Mn)(As,P) thin films, the disorder caused by doping of Mn impurities and the defects due to the low-temperature growth affect the optical properties. This effect is taken into account within the Born approximation by including the lifetime broadening of quasiparticle spectral functions in evaluating the Kubo formula.[24,49] The lifetime broadening $\hbar\gamma$ is taken as a constant value equal to 100 meV in accordance with that used in Ref. 50. In this paper, we restrict our attention to the $T = 0$ limit, which allows to neglect scattering of VB quasiparticles off thermal fluctuations in the Mn moments orientation.

Once the frequency-dependent dielectric functions are obtained, the Kerr-angle spectra are calculated.[48] In the polar geometry, where the z-axis is chosen to be perpendicular to the solid surface, and parallel to the magnetization direction and taking into account all effects of propagation and reflections in a thin (Ga,Mn)(As,P) layer onto a GaAs substrate, the expression for the complex Kerr angle for a layer of finite thickness can be obtained from the amplitude reflexion coefficients for left and right circular polarization[48,51]

$$r^{\pm} = \frac{r_{01}^{\pm} + r_{12}^{\pm}\exp\left(i\phi^{\pm}\right)}{1 + r_{01}^{\pm}r_{12}^{\pm}\exp\left[i\phi^{\pm}\right]}, \tag{2}$$

where indices 0, 1, and 2 refer to the vacuum, the magnetic layer, and the substrate, respectively. The amplitude reflection coefficients are $r_{ij}^{\pm} = (n_i^{\pm} - n_j^{\pm})/(n_i^{\pm} + n_j^{\pm})$. The optical absorption and dephasing inside the magnetic layer are given by $\phi^{\pm} = 4\pi n_1^{\pm}d/\lambda$ with d the layer thickness, λ the optical wavelength, and $(n_1^{\pm})^2 = (\varepsilon_{xx} \pm i\,\varepsilon_{xy})$ the indices for the eigenmodes. One has $n_0^{\pm} = 1$ for the vacuum and $n_2^{\pm} = n_s$ for the substrate. For small Kerr rotation angle θ_K and

ellipticity η_K, the complex rotation angle is $\theta_K + i\,\eta_K = i(r^+ - r^-)/(r^+ + r^-)$. Keeping terms to the first order in ε_{xy} and taking into account that the reflection coefficient r_{12} at the layer/substrate interface is very small (typically less than 1%), the complex rotation angle can be written as

$$\theta_K + i\,\eta_K = \frac{\varepsilon_{xy}(\exp(i\phi) - 1)}{\sqrt{\varepsilon_{xx}}(\varepsilon_{xx} - 1)}(1 + r)\,, \tag{3}$$

where $r = 2r_{12}\exp(i\phi)(\frac{\varepsilon_{xx}+1}{\varepsilon_{xx}-1} + \frac{i\,\phi}{\exp(i\phi)-1})$, and $\phi = 4\pi nd/\lambda$ is the complex optical phase with $n^2 = (\eta + i\,\kappa)^2 = \varepsilon_{xx}$.

B. Dielectric functions

The calculated real and imaginary parts of the dielectric functions for photon energy ranging up to 6 eV are shown in Figs. 3(a)–3(d) for samples A, B, and C with close effective Mn concentrations and different P compositions: $y = 0\%$, 7.0%, and 11.3%, respectively. For sample A with in-plane easy axis, the magnetization was assumed to be tilted perpendicular to the plane by a magnetic field whose effect on the substrate was neglected.

We first discuss the role of the P fraction in the frequency-dependent dielectric tensor (Fig. 3). The first positive peak of the real part of ε_{xx} can be attributed to the interband transitions ($\Gamma_8^V \rightarrow \Gamma_6^C$) around the E_0 critical point. As can be seen in the inset of Fig. 3(b), E_0 increases with increasing P fraction y. These observations are consistent with previous theoretical studies.[37] Like the fundamental band gap, the dielectric constant in the static limit, $\varepsilon(0)$, is a very important physical quantity for SCs. Let us note the ability of our model to predict the correct $\varepsilon(0)$ value in SCs. Fig. 3(b) shows that $\varepsilon(0)$ decreases as a function of y content. This behavior can be explained by an important alloying effect. The present calculation gives $\varepsilon(0) = 10.10$ for $y = 0.0$, 9.63 for $y = 0.07$, and 9.57 for $y = 0.113$. Generally speaking, these values of $\varepsilon(0)$ are consistent with the experimental ones for GaAs ($\varepsilon(0) = 10.9$ (Ref. 52)) and GaP ($\varepsilon(0) = 9.1$ (Ref. 53)). The imaginary parts of ε_{xx} functions for the three samples shown in Fig. 3(a) are characterized by two major interband-transition structures, E_1 and E_2. The E_1 interband-transition structure located at about 3 eV is assigned to direct interband transitions along the $\Lambda\,(\Gamma - L)$ direction in face-centered cubic zinc-blende SCs, where the heavy-hole VBs disperse quite parallel to the conduction band.[54] The interband-transition structure E_1 in GaAs is located at 3 eV, where the corresponding structure in GaP is located at about 3.7 eV indicating that the evolution of the 3-eV structure of $(Ga_{1-x}Mn_x)(As_{1-y}P_y)$ arises from the energy shifts of the E_1 transition edges from GaAs to GaP by alloying. The E_2 edge located at about 5 eV is assigned to transitions near the X and Σ points designated as $E_2'(X)$ and $E_2(\Sigma)$, respectively.[55] We also interpret the evolution of the 5 eV structure as due to the alloying effect.

As can be seen from Eq. (3), the MOKE signal is proportional to the off-diagonal component of the magneto-optical dielectric tensor ε_{xy}. In Figs. 3(c) and 3(d), we show, respectively, the imaginary and real parts of ε_{xy} as a function of photon energy for samples A, B, and C. The structure at about 1.6 eV (Fig. 3(c)) is related to the onset of absorption spectra for circular σ_+ and σ_- polarizations shown in Fig. 4 with a main contribution from the light-hole bands. The 2 eV structure can be traced back to the maximum difference of σ_+ and σ_- absorption spectra shown in Fig. 4. These structures originate from the giant Zeeman splitting of the Γ_8^V

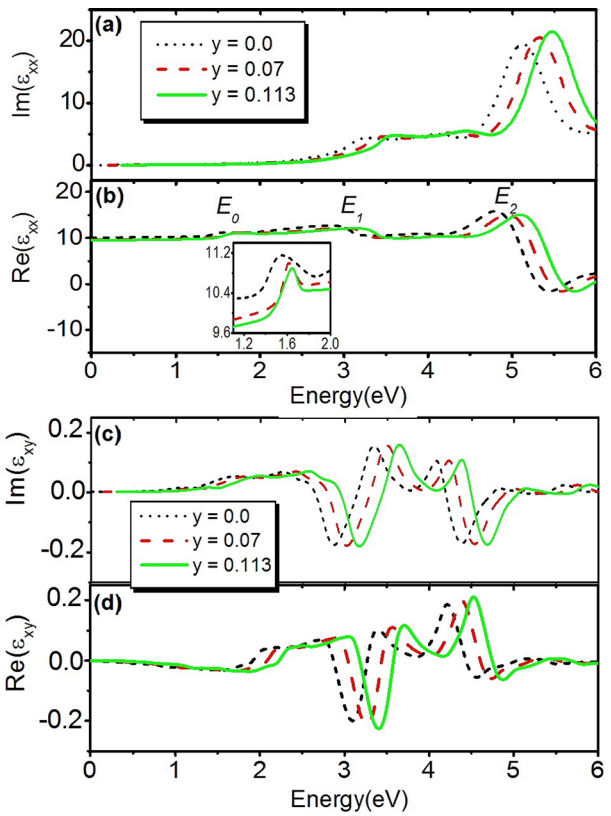

FIG. 3. Calculated energy-dependent complex dielectric functions Im (ε_{xx}) (a), Re (ε_{xx}) (b), Im (ε_{xy}) (c), and Re (ε_{xy}) (d) for samples A, B, and C with phosphorus fractions y = 0 (black dotted line), y = 0.07 (red dashed line), and y = 0.113 (green full line), respectively. The inset in (b) shows a zoom of Re (ε_{xx}) at the band gap. The sign of Re (ε_{xy}) and Im (ε_{xy}) depends on the orientation of the magnetization. Here, it is oriented in the $+z$-direction taken along the wave vector of incident light.

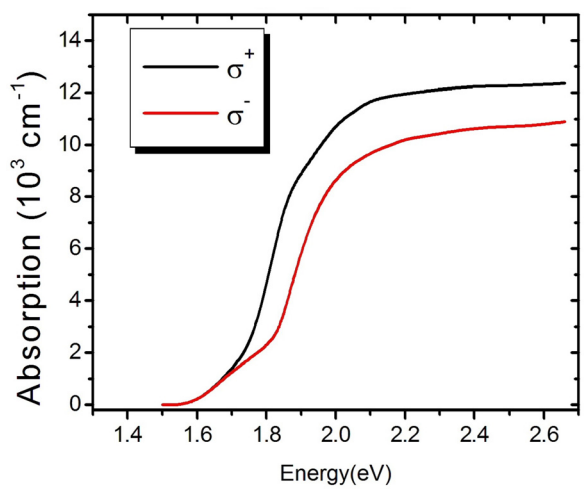

FIG. 4. Calculated absorption for circular σ_+ and σ_- polarizations taking into account the upper six valence bands for sample B ($x_{\text{eff}} = 3.8\%$, $y = 7\,\%$).

VBs in the presence of the *p-d* exchange interaction between the holes and the Mn spins.

C. MOKE spectra

We now consider the MOKE spectra and compare the experimental and theoretical curves. The MOKE measurements were performed in polar geometry with the incident light beam quasi-normal to the sample surface. The sample was illuminated with light from a 150 W Xe lamp passing through a monochromator. Light with selected wavelength was polarized with a Glan-Thompson polarizer. The linearly polarized light was modulated by a mechanical chopper and a photo-elastic modulator (PEM), at $f_0 = 250$ Hz and $f = 50$ kHz, respectively. The polarizer axis was oriented at 45° with respect to the modulator axes. After reflection on the sample, the light beam passed through an analyzer aligned with one of the modulator axes and its intensity was detected with a Si photodiode. The detected signal was fed into two lock-in amplifiers referenced to the chopper frequency (f_0) and to the PEM frequency f for the Kerr ellipticity and $2f$ for the Kerr rotation angle. A 20 mT external magnetic field B was applied perpendicular to the sample surface in order to saturate the magnetization and the MOKE spectra were then measured for $+B$ and $-B$. Only samples with perpendicular easy axis were studied. The Kerr rotation and ellipticity were then obtained from the difference of the signals for $+B$ and $-B$ divided by the incident intensity at f_0, taking carefully into account the Bessel functions in the development of the signal in Fourier series.[56] The sample temperature was varied between 10 K and the Curie temperature in a closed-cycle liquid helium cryostat. As an example, Figs. 5(a) and 5(b) show the temperature dependence of the Kerr rotation angle and ellipticity, respectively, for sample B. Both signals decrease with increasing temperature and vanish at $T = 80$ K close to the Curie temperature of the sample (see Fig. 1(a)). Experimental data at $T = 10$ K are now compared to the theoretical results.

In Fig. 6, we show the calculated and experimental MOKE spectra of samples B and C with close effective Mn concentrations and different P concentrations: $y = 7\%$ and $y = 11.3\%$, respectively. The magnetic easy axis is in both cases perpendicular to the layer. The spectral shapes of the Kerr rotation angle and ellipticity of the two samples have common characteristics indicating that the P fraction does not strongly affect the MOKE spectra. Indeed, the principal features for relevant energies are present for both P concentrations. The Kerr rotation angle shows only a very broad

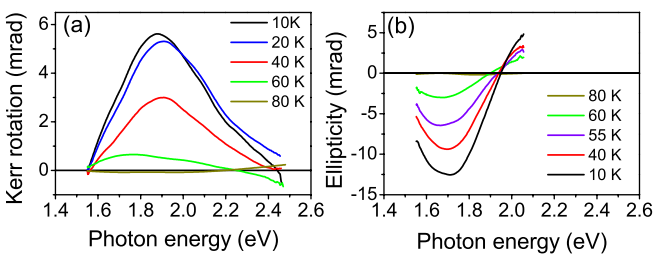

FIG. 5. Temperature dependence of the Kerr rotation angle (a) and ellipticity (b) for sample B ($x_{\text{eff}} = 3.8\%$, $y = 7\,\%$).

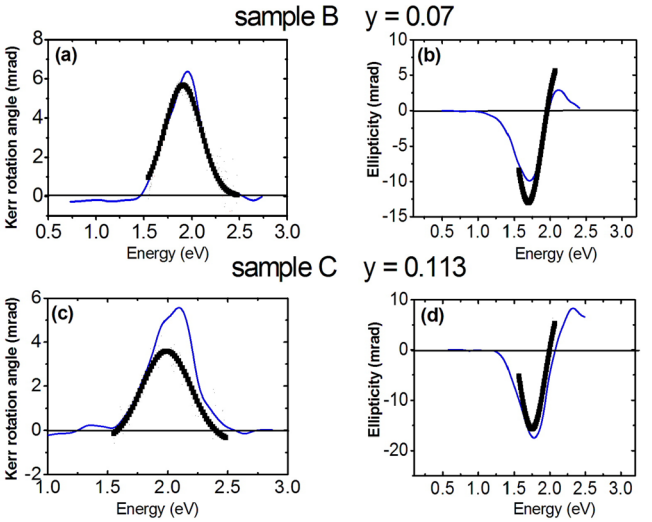

FIG. 6. MOKE spectra of samples B and C: rotation angle (left panel) and ellipticity (right panel). The theoretical results are represented by solid lines. The solid symbols show the experimental data at T = 10 K.

positive signal in the whole energy range 1.5–2.5 eV, while the ellipticity shows negative and positive contributions. The ellipticity spectra show a negative peak around 1.8 eV. Its magnitude decreases to zero around 2.0 eV. The observed MOKE spectrum of these samples can be well explained in terms of optical transitions between the VBs and conduction band. The Kerr rotation angle shows a value of the order of 5 mrad ($\simeq 0.3°$) whereas the ellipticity is in the range of 15 mrad. These values are consistent with previous reports in (Ga,Mn)As compounds.[25,26,29,30,32,57] Let us note however that their respective amplitudes depend on the layer thickness (Eq. (3)). This can be clearly seen from the following expressions of θ_K and η_K obtained neglecting absorption (which is weak in these magnetic SCs where $\kappa \ll \eta$), and taking $\epsilon_{xy} = \epsilon'_{xy} + i\epsilon''_{xy}$: $\theta_K = [\epsilon'_{xy}(\cos\phi - 1) - \epsilon''_{xy}\sin\phi]/(\eta(\eta^2 - 1))$ and $\eta_K = [\epsilon''_{xy}(\cos\phi - 1) + \epsilon'_{xy}\sin\phi]/(\eta(\eta^2 - 1))$ where $\phi = 4\pi\eta d/\lambda$. This opens the possibility to optimize one of these two quantities by an appropriate choice of the layer thickness, for instance in order to improve the detection in time-resolved pump-probe experiments based on MOKE, which has not been considered up to now.

To summarize, as can be seen in Fig. 6, the effect of the increase of the P fraction from 7% to 11.3% leads to a slight decrease in the Kerr rotation angle, an increase in the ellipticity, and a slight blueshift of the two spectra.

An overall good agreement between microscopic calculations and experiment data is obtained. Not only the spectral shape but also the energy positions of the peaks are well reproduced by the theoretical model. However, there are small discrepancies between the theory and experiment regarding the magnitude, which might be explained by alloying effects.

We further investigate the effect of the Mn content in the MOKE spectra. Figure 7 shows the experimental and theoretical Kerr rotation angle (Fig. 7(a)) and ellipticity (Fig. 7(b)) for samples C and D. These samples have the same P concentration of 7% but different Mn concentrations. The overall trend as a function of photon energy is the same for samples C and

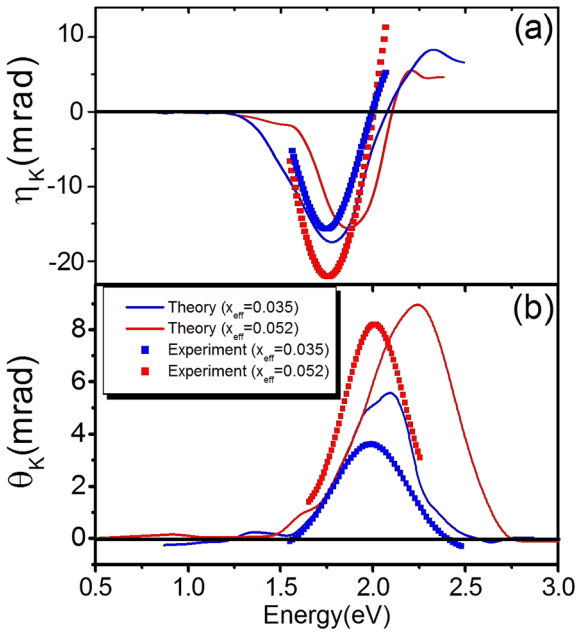

FIG. 7. Calculated Kerr ellipticity (a) and rotation angle (b) for samples with two different Mn contents; **C** ($x_{\text{eff}} = 3.5\%$) and **D** ($x_{\text{eff}} = 5.2\%$)) and the same P concentration, $y = 11.3\%$. The layer thickness is taken as 55 nm.

D. However, the amplitude and position of the main peak sensitively depend on the Mn content. The experimental Kerr-angle peak near 2.0 eV (Fig. 7(b)) shifts to a higher energy by ≈60 meV and its amplitude increases by 100% with increasing Mn doping from $x_{\text{eff}} = 3.5\%$ to 5.2%. The calculated Kerr-angle peak also shows a blue shift and an increase in amplitude (≈150 meV shift and 60% amplitude increase). The ellipticity spectra (Fig. 7(a)) depend less strongly on the Mn fraction, both experimentally and theoretically. The peak energy shift, which is found larger for theoretical curves than for experimental ones, could be adjusted by changing the valence band splitting parameter B_G. Generally speaking, these observations are consistent with the previous studies of (Ga,Mn)As ternary alloys where several authors have reported a moderate dependence of the MO properties on the Mn concentration.[11,25,26,30,31,34]

It is worth mentioning that the spectral dependence of the magneto-optical Kerr effect obtained using the 40-band **k.p** model in (Ga,Mn)(As,P) is in much better agreement with experimental results than in ternary (Ga,Mn)As using the 30-band **k.p** model.[30] We believe that the more accurate description of the MOKE originates from a better description of the bands with our 40-band **k.p** model in particular, from a good determination of the BS details over a wide range of k-vectors in four directions.

To conclude, let us recall that the position of the Fermi level in ferromagnetic (III, Mn)V is still a matter of debate. There are two alternative VB pictures in (Ga,Mn)As. The first scenario predicts a merger of the Mn impurity band with the host VB considering that *p-d* exchange interaction between the delocalized VB holes and the localized d-electrons of Mn^{2+} ions is the main origin of the ferromagnetic order. According to this model, the Fermi energy lies within the SC VB and is determined by the hole carrier density.[41,58–60] Competing with this hypothesis, the impurity-band model predicts that the Fermi level resides inside the Mn impurity band detached from the GaAs VB.[14–16,61–63] In this case, the ferromagnetism spreads within this impurity band by a hopping effect without affecting the VB holes. In our approach, we have assumed that the Fermi level is located within the VB. The good agreement between theoretical and experimental magneto-optical Kerr spectra is consistent with this energy scheme although we cannot definitely rule out the alternative picture. Our results are also consistent with the previous experimental and theoretical reports for high quality $Ga_{1-x}Mn_xAs$ ferromagnetic layers.[64]

IV. CONCLUSION

This work is the first comparative experimental/theoretical study of both Kerr rotation and ellipticity on ferromagnetic $Ga_{1-x}Mn_xAs_{1-y}P_y$/GaAs epilayers. We have presented a theoretical modeling of electronic and MO properties of GaMnAsP layer using the mean-field approximation and the 40-band **k.p** model, in which the BS, the complex dielectric function, the Kerr rotation, and the ellipticity spectra are calculated in the interband transition region. We have considered the effect of the phosphorus and Mn compositions on the spectral dependence of the magneto-optical Kerr effect. The present model accurately reproduces the experimental MOKE spectra, as well as the dependence of the Kerr angle and ellipticity on P and Mn contents. This study demonstrates that the P incorporation has little effect on MOKE in such quaternary alloys within the alloying range 0%–11%. However, the main peak in the Kerr rotation and ellipticity angle shows a significant variation in magnitude as well as a slight shift as a function of the Mn fraction. Our results provide guidelines for tuning the magneto-optical properties of (Ga,Mn)(As,P) alloys.

ACKNOWLEDGMENTS

We thank A. Maitre for the Hall measurements. This work was financially supported by the PHC Utique program of the French Ministry of Foreign Affairs and Ministry of Higher Education and Research and the Tunisian Ministry of Higher Education and Scientific Research in the CMCU project number 16G1303, by the French Agence Nationale de la Recherche (ANR13-JS04-0001-01), and by the French RENATECH network. M.Y. and H.R. acknowledge financial support from the Tunisian Ministry of Higher Education and Scientific Research.

[1]A. Lemaître, A. Miard, L. Travers, O. Mauguin, L. Largeau, C. Gourdon, V. Jeudy, M. Tran, and J.-M. George, Appl. Phys. Lett. **93**, 021123 (2008).
[2]M. Cubukcu, H. J. von Bardeleben, K. Khazen, J. L. Cantin, O. Mauguin, L. Largeau, and A. Lemaître, Phys. Rev. B **81**, 041202 (2010).
[3]P. Stone, K. Alberi, S. Tardif, J. Beeman, K. Yu, W. Walukiewicz, and O. Dubon, Phys. Rev. Lett. **101**, 087203 (2008).
[4]J. Mašek, J. Kudrnovský, F. Máca, J. Sinova, A. MacDonald, R. Campion, B. Gallagher, and T. Jungwirth, Phys. Rev. B **75**, 045202 (2007).
[5]L. Thevenard, C. Gourdon, J. Y. Prieur, H. J. von Bardeleben, S. Vincent, L. Becerra, L. Largeau, and J.-Y. Duquesne, Phys. Rev. B **90**, 094401 (2014).
[6]N. Tesařová, D. Butkovičová, R. P. Campion, A. W. Rushforth, K. W. Edmonds, P. Wadley, B. L. Gallagher, E. Schmoranzerová, F. Trojánek, P.

Malý, P. Motloch, V. Novák, T. Jungwirth, and P. Němec, Phys. Rev. B **90**, 155203 (2014).
[7]S. Haghgoo, M. Cubukcu, H. J. von Bardeleben, L. Thevenard, A. Lemaître, and C. Gourdon, Phys. Rev. B **82**, 041301 (2010).
[8]H. Ebert, Rep. Prog. Phys. **59**, 1665 (1996).
[9]W. Reim and J. Schoenes, *Ferromagnetic Materials* (North-Holland Publishing, 1988), Vol. 5.
[10]V. N. Antonov, A. N. Yaresko, A. Y. Perlov, V. V. Nemoshkalenko, P. M. Oppeneer, and H. Eschrig, Low Temp. Phys. **25**, 387 (1999).
[11]B. C. Chapler, R. C. Myers, S. Mack, A. Frenzel, B. C. Pursley, K. S. Burch, E. J. Singley, A. M. Dattelbaum, N. Samarth, D. D. Awschalom, and D. N. Basov, Phys. Rev. B **84**, 081203 (2011).
[12]K. Burch, D. Awschalom, and D. Basov, J. Magn. Magn. Mater. **320**, 3207 (2008).
[13]R. Chakarvorty, S. Shen, K. J. Yee, T. Wojtowicz, R. Jakiela, A. Barcz, X. Liu, J. K. Furdyna, and M. Dobrowolska, Appl. Phys. Lett. **91**, 171118 (2007).
[14]K. Ando, H. Saito, K. C. Agarwal, M. C. Debnath, and V. Zayets, Phys. Rev. Lett. **100**, 067204 (2008).
[15]M. Berciu, R. Chakarvorty, Y. Zhou, M. Alam, K. Traudt, R. Jakiela, A. Barcz, T. Wojtowicz, X. Liu, J. Furdyna, and M. Dobrowolska, Phys. Rev. Lett. **102**, 247202 (2009).
[16]M. Dobrowolska, K. Tivakornsasithorn, X. Liu, J. K. Furdyna, M. Berciu, K. M. Yu, and W. Walukiewicz, Nat. Mater. **11**, 444 (2012).
[17]G. P. Moore, J. Ferré, A. Mougin, M. Moreno, and L. Däweritz, J. Appl. Phys. **94**, 4530 (2003).
[18]S. Shihab, H. Riahi, L. Thevenard, H. J. von Bardeleben, A. Lemaître, and C. Gourdon, Appl. Phys. Lett. **106**, 142408 (2015).
[19]D. Wang, Y. Ren, X. Liu, J. Furdyna, M. Grimsditch, and R. Merlin, Phys. Rev. B **75**, 233308 (2007).
[20]A. Dourlat, V. Jeudy, C. Testelin, F. Bernardot, K. Khazen, C. Gourdon, L. Thevenard, L. Largeau, O. Mauguin, and A. Lemaître, J. Appl. Phys. **102**, 023913 (2007).
[21]L. Herrera Diez, R. K. Kremer, A. Enders, M. Rössle, E. Arac, J. Honolka, K. Kern, E. Placidi, and F. Arciprete, Phys. Rev. B **78**, 155310 (2008).
[22]A. Dourlat, V. Jeudy, A. Lemaître, and C. Gourdon, Phys. Rev. B **78**, 161303(R) (2008).
[23]D. Hrabovsky, E. Vanelle, A. R. Fert, D. S. Yee, J. P. Redoules, J. Sadowski, J. Kanski, and L. Ilver, Appl. Phys. Lett. **81**, 2806 (2002).
[24]J. Sinova, T. Jungwirth, J. Kučera, and A. H. MacDonald, Phys. Rev. B **67**, 235203 (2003).
[25]R. Lang, A. Winter, H. Pascher, H. Krenn, X. Liu, and J. Furdyna, Phys. Rev. B **72**, 024430 (2005).
[26]S. Picozzi, A. Continenza, M. Kim, and A. J. Freeman, Phys. Rev. B **73**, 235207 (2006).
[27]M.-H. Kim, G. Acbas, M.-H. Yang, I. Ohkubo, H. Christen, D. Mandrus, M. A. Scarpulla, O. D. Dubon, Z. Schlesinger, P. Khalifah, and J. Cerne, Phys. Rev. B **75**, 214416 (2007).
[28]M. Turek, J. Siewert, and J. Fabian, Phys. Rev. B **80**, 161201 (2009).
[29]G. Acbas, M.-H. Kim, M. Cukr, V. Novák, M. A. Scarpulla, O. D. Dubon, T. Jungwirth, J. Sinova, and J. Cerne, Phys. Rev. Lett. **103**, 137201 (2009).
[30]C. Sun, J. Kono, Y. H. Cho, A. K. Wójcik, A. Belyanin, and H. Munekata, Phys. Rev. B **83**, 125206 (2011).
[31]H. Terada, S. Ohya, and M. Tanaka, Appl. Phys. Lett. **106**, 222406 (2015).
[32]A. V. Kimel, G. V. Astakhov, A. Kirilyuk, G. M. Schott, G. Karczewski, W. Ossau, G. Schmidt, L. W. Molenkamp, and T. Rasing, Phys. Rev. Lett. **94**, 227203 (2005).
[33]B. Al-Qadi, N. Nishizawa, K. Nishibayashi, M. Kaneko, and H. Munekata, Appl. Phys. Lett. **100**, 222410 (2012).
[34]N. Tesařová, T. Ostatnický, V. Novák, K. Olejník, J. Šubrt, H. Reichlová, C. T. Ellis, A. Mukherjee, J. Lee, G. M. Sipahi, J. Sinova, J. Hamrle, T. Jungwirth, P. Němec, J. Černe, and K. Výborný, Phys. Rev. B **89**, 085203 (2014).
[35]I. Saidi, S. Ben Radhia, and K. Boujdaria, J. Appl. Phys. **107**, 043701 (2010).
[36]M. Yahyaoui, C. Testelin, C. Gourdon, and K. Boujdaria, J. Appl. Phys. **111**, 033902 (2012).
[37]M. Yahyaoui, K. Boujdaria, M. Cubukcu, C. Testelin, and C. Gourdon, J. Phys.: Condens. Matter **25**, 346001 (2013).
[38]T. Dietl, H. Ohno, and F. Matsukura, Phys. Rev. B **63**, 195205 (2001).
[39]M. Cubukcu, H. J. von Bardeleben, J. L. Cantin, and A. Lemaître, Appl. Phys. Lett. **96**, 102502 (2010).
[40]R. Neffati, I. Saidi, and K. Boujdaria, J. Appl. Phys. **112**, 053716 (2012).
[41]T. Dietl, Science **287**, 1019 (2000).
[42]G. E. Pikus and G. L. Bir, Sov. Phys. Solid. State **1**, 1502 (1960) [Fiz. Tverd. Tela (Leningrad) **1**, 1642 (1959) (in Russian)]); see also, G. L. Bir and G. E. Pikus, *Symmetry and Strain-Induced Effects in Semiconductors* (Wiley, New York, 1974).
[43]K. F. Berggren and B. E. Sernelius, Phys. Rev. B **24**, 1971 (1981).
[44]B. E. Sernelius, Phys. Rev. B **34**, 5610 (1986).
[45]Y. Zhang and S. Das Sarma, Phys. Rev. B **72**, 125303 (2005).
[46]S. C. Jain, J. M. McGregor, and D. J. Roulston, J. Appl. Phys. **68**, 3747 (1990).
[47]T. Jungwirth, P. Horodyská, N. Tesařová, P. Němec, J. Šubrt, P. Malý, P. Kužel, C. Kadlec, J. Mašek, I. Němec, M. Orlita, V. Novák, K. Olejník, Z. Šobáň, P. Vašek, P. Svoboda, and J. Sinova, Phys. Rev. Lett. **105**, 227201 (2010) and supplemental at http://link.aps.org/supplemental/10.1103/PhysRevLett.105.227201.
[48]A. K. Zvezdin and V. A. Kotov, *Modern Magneto-Optics and Magneto-Optical Materials* (CRC Press, New York, 1997).
[49]J. Sinova, T. Jungwirth, S.-R. E. Yang, J. Kučera, and A. H. MacDonald, Phys. Rev. B **66**, 041202 (2002).
[50]T. Jungwirth, M. Abolfath, J. Sinova, J. Kučera, and A. H. MacDonald, Appl. Phys. Lett. **81**, 4029 (2002).
[51]The + and − signs refer to the left and right circular polarization $e_+ = x + iy$, $e_+ = x - iy$, respectively in the (x, y, z) reference frame with z along the incident wave vector of light. The definition of Kerr rotation angle θ_K and ellipticity η_K is such that rotation and ellipticity are positive (anti-clockwise rotation) in the (x,y,z) frame when the observer faces the incoming light.
[52]E. Burstein, M. H. Brodsky, and G. Lucovsky, Int. J. Quantum Chem. **1**, 759 (1967).
[53]A. S. Barker, Phys. Rev. **165**, 917 (1968).
[54]P. Lautenschlager, M. Garriga, S. Logothetidis, and M. Cardona, Phys. Rev. B **35**, 9174 (1987).
[55]M. L. Cohen and J. R. Chelikowsky, *Electronic Structure and Optical Properties of Semiconductors* (Springer, Berlin, 1988).
[56]K. Sato, Jpn. J. Appl. Phys., Part 1 **20**, 2403 (1981).
[57]H. Riahi, L. Thevenard, M. Maaref, B. Gallas, A. Lemaître, and C. Gourdon, J. Magn. Magn. Mater. **395**, 340 (2015).
[58]T. Jungwirth, J. Mašek, J. Kučera, and A. H. MacDonald, Rev. Mod. Phys. **78**, 809 (2006).
[59]M. Elsen, H. Jaffrès, R. Mattana, M. Tran, J.-M. George, A. Miard, and A. Lemaître, Phys. Rev. Lett. **99**, 127203 (2007).
[60]D. Neumaier, M. Turek, U. Wurstbauer, A. Vogl, M. Utz, W. Wegscheider, and D. Weiss, Phys. Rev. Lett. **103**, 087203 (2009).
[61]K. S. Burch, J. Stephens, R. K. Kawakami, D. D. Awschalom, and D. N. Basov, Phys. Rev. B **70**, 205208 (2004).
[62]J.-M. Tang and M. E. Flatté, Phys. Rev. Lett. **101**, 157203 (2008).
[63]M. Kobayashi, I. Muneta, Y. Takeda, Y. Harada, A. Fujimori, J. Krempaský, T. Schmitt, S. Ohya, M. Tanaka, M. Oshima, and V. N. Strocov, Phys. Rev. B **89**, 205204 (2014).
[64]P. Němec, V. Novák, N. Tesařová, E. Rozkotová, H. Reichlová, D. Butkovičová, F. Trojánek, K. Olejník, P. Malý, R. P. Campion, B. L. Gallagher, J. Sinova, and T. Jungwirth, Nat. Commun. **4**, 1422 (2013).